Applied Energy 138 (2015) 11–20

Contents lists available at ScienceDirect

Applied Energy

journal homepage: www.elsevier.com/locate/apenergy

Theoretical and experimental investigation of the Miller cycle diesel engine in terms of performance and emission parameters

Guven Gonca [a,*], Bahri Sahin [a], Adnan Parlak [b], Yasin Ust [a], Vezir Ayhan [c], İdris Cesur [c], Barış Boru [c]

[a] Yildiz Technical University, Naval Arch. and Marine Eng. Depart, Besiktas, Istanbul, Turkey
[b] Yildiz Technical University, Marine Eng. Depart, Besiktas, Istanbul, Turkey
[c] Sakarya University, Technical Education Faculty, Sakarya, Turkey

HIGHLIGHTS

- Miller cycle is applied to a DI diesel engine to decrease NOx emissions.
- Emission and performance parameters are calculated by two-zone combustion model.
- Theoretical model is verified with the experimental results.

ARTICLE INFO

Article history:
Received 14 February 2014
Received in revised form 25 July 2014
Accepted 16 October 2014
Available online 7 November 2014

Keywords:
Diesel engine
Miller cycle
Performance
Emission
Two-zone combustion model

ABSTRACT

Pollutant exhaust emissions, particularly NOx, produced by diesel engines must be reduced to limit values defined by the environmental regulations as the emissions have many harmful influences on the environment. Recently, the application of the Miller cycle into the internal combustion engines has been proposed to abate NOx emissions. In the present study, the Miller cycle with late intake valve closing (LIVC) version is applied into a single cylinder, four-stroke, direct injection, naturally aspirated diesel engine. Three different cam shafts have been manufactured to provide 5, 10 and 15 crank angle (CA) retarding compared to original camshaft. The optimum retarding angle has been determined as 5 CA in terms of NOx reduction. The attained results have been compared with conventional diesel engine which has standard CA (0 crank angle retarding) in point of the performance and NO, HC, CO emissions. In order to provide a model validation for engine torque, brake power, brake efficiency, specific fuel consumption (SFC) and NO, the Miller cycle diesel engine is modeled by using two-zone combustion model for 5 CA retarding at full load conditions. The simulation results have been verified with experimental data with non-considerable errors. In the experimental results, NO emissions decreased by 30% with 2.5% power loss and a remarkable change is not seen in the HC, CO emissions. The results show that the method could be easily applied into the diesel engine in order to minimize NO emissions.

1. Introduction

It is well known that diesel engines produce NOx emissions in higher concentration compared to Otto cycle engines and gas turbines due to higher combustion temperatures. Recently, application of the Miller cycle into the internal combustion engines has been proposed to decrease the NOx emissions by the engine researchers. The Miller cycle is based on that reducing the compression ratio compared to the expansion ratio by closing intake valve much time later from the bottom dead center (BDC), which is called late intake valve closing (LIVC) version, or the Miller cycle condition can be obtained by closing intake valve during the period of suction before piston reaches to the BDC, which is called early intake valve closing (EIVC) version. The goal is to decrease combustion temperatures and also NOx emissions.

In the literature, various parametric studies on the air standard Miller cycle have been carried out to understand the effect of the cycle on the performance based on thermodynamics. Sarkhi et al. [1] analyzed the cycle performance by using the maximum power density criteria and showed graphically the effects of parameters on the cycle. Sarkhi et al. [2,3] investigated the impacts of the variable specific heats of the working fluid on the performance for an air standard reversible Miller cycle [2] and irreversible Miller cycle [3]. Zhao and Chen [4] conducted a performance analysis for an-air standard irreversible Miller cycle. It was shown that the power

* Corresponding author. Tel.: +90 212 383 2950; fax: +90 212 383 2941.
E-mail address: ggonca@yildiz.edu.tr (G. Gonca).

http://dx.doi.org/10.1016/j.apenergy.2014.10.043
0306-2619/

Nomenclature

A	heat transfer area (cm^2)
B	bore (cm)
C_v	specific heat at constant volume (kJ/kg K)
C_p	specific heat at constant pressure (kJ/kg K)
C	blow by coefficient
ECP	equilibrium combustion products
F	fuel–air ratio
h	specific enthalpy (kJ/kg)
h_{tr}	heat transfer coefficient (W/m^2 K) of burned and unburned zones
H	enthalpy (kJ/kg)
H_u	lower heat value of the fuel (kJ/kg)
m	mass (g)
$\dot{m}$	time- dependent mass rate (g/s)
M	molecular weight (g)
n	injection constant
P	pressure (bar)
Q	heat loss to the cylinder wall (J)
$\dot{Q}$	rate of heat transfer (J/s)
RGF	residual gas fraction
s	specific entropy (kJ/kg K)
S	stroke (cm)
SFC	specific fuel consumption
T	temperature (K)
u	specific internal energy (kJ/kg)
v	specific volume (cm^3/g)
V	volume (cm^3)
W	work output (J)
x	mass fraction burned
$\dot{x}_i$	fraction rate of the total injected fuel mass

Greek letters

ε	ratio of half stroke to rod length
ϕ	equivalence ratio
$\Gamma(n)$	gamma function
θ	crank angle (degree)
τ	time (ms)
ω	angular velocity (rad/s)

Subscripts

a	air
b	burned zone
cyl	cylinder
di	injection duration parameter
dif	diffusive combustion phase
f	fuel
fi	injected fuel
id	ignition delay (ms)
l	leak, loss
me	mean
n	net
pre	premixed combustion phase
r	reference
s	stoichiometric
si	start of fuel injection (degree)
u	unburned zone
w	cylinder walls

output and thermal efficiency of the Miller cycle are higher than those of the Otto and Atkinson cycle. Wu et al. [5] performed a simulation to apply the Miller cycle into a supercharged Otto engine and an increment was seen in the work output of the engine. Lin and Hou [6] stated that, at the same maximum temperature conditions, the Miller cycle had a superiority compared to Otto cycle in terms of the performance. Ebrahimi [7] analyzed an air standard reversible Miller cycle with respect to variation of engine speed and variable specific heat ratio of working fluid and Ebrahimi [8] analyzed an air standard irreversible Miller cycle with respect to the variation of relative air–fuel ratio and stroke length based on finite-time thermodynamics. The power output and thermal efficiency were attained by introducing the compression ratio, air–fuel ratio and stroke length. It was illustrated that the power output and thermal efficiency of the cycle reached to maximum point with certain values of the compression ratio. Gonca et al. [9,10] presented the performance maps for Dual-Miller cycle (DMC) and showed that the maximum cycle temperature and so NOx emissions could be decreased by applying the Miller cycle to a diesel engine.

Some researchers applied the Miller cycle into gasoline and Otto cycle natural gas engines and they achieved to abate the NOx emissions. Wang et al. [11,12] carried out experimental [11] and analytical [12] studies to examine the influences of the application of the Miller cycle into a gasoline engine. The results indicated that the gasoline engine operating with the Miller cycle led to considerably decreasing of NOx emissions by lowering the combustion temperatures. Mikalsen et al. [13] investigated the feasibility and potential advantages of the application of the Miller cycle into a small scale Otto cycle natural gas engine by using multidimensional simulation for a combined heat and power system. As a result, the NOx emissions and specific fuel consumption (SFC) of the engine were reduced with the cost of a decreased power to weight ratio. Kesgin [14] performed an experimental and theoretical study in order to examine the influence of the application of the Miller cycle into a natural gas engine. The results showed that the efficiency could be increased and NOx emissions could be decreased. Li et al. [15] experimentally examined the influences of the Miller cycle with the EIVC and LIVC versions on the brake specific fuel consumption (BSFC) of a boosted direct injection (DI) gasoline engine. At the high load conditions, the fuel economy is improved up to 4.7% with LIVC; however, a considerable change was not seen in SFC with EIVC. At the low load conditions, SFC is improved up to 6.8% and 7.4% with LIVC and EIVC, respectively.

The application of the Miller cycle into the Diesel engines has been recently proposed to decrease NOx emissions. Wang et al. [16] achieved the reduction of NOx emissions by experimentally applying the Miller cycle into a diesel engine. Gonca et al. [17–19] computationally demonstrated that the application of Miller cycle into a diesel engine could abate the NO emissions and increase the brake efficiency. Rinaldini et al. [20] carried out an experimental and numerical study by using KIVA which is a CFD based code. They assessed the potential and the limits of the Miller cycle application to a High Speed Direct Injection (HSDI) Diesel engines in terms of abating NOx and soot. It was shown in the results that when the Miller cycle applied into a diesel engine, NOx and soot emissions could be reduced up to 25% and 60%, respectively.

In the present study, apart from former studies, the influences of the Miller cycle application with LIVC version on the performance and emission parameters of a single cylinder diesel engine have been experimentally and theoretically investigated by using two-zone combustion model. The torque, brake power and efficiency, SFC, in-cylinder pressure and temperature, NO, CO and

HC emissions have been experimentally obtained. The experimental results have been compared with the theoretical results and a good agreement have been acquired between the theoretical and experimental results. In the literature, even though there is an experimental study using EIVC version [16], there is no such a study examining the Miller cycle diesel engine with LIVC version by experiments. This is the most important originality and also two-zone combustion model is used to obtain model validation along with the experiments. Hence, this study has a good novelty and originality.

2. Materials and methods

2.1. Experimental set-up

The experiments were conducted with a single cylinder, naturally aspirated, four-stroke and direct injection (DI) diesel engine. Table 1 demonstrates the engine properties. The Miller cycles were realized by retarding the intake valve closing as 5, 10 and 15 CA. The original camshaft was camshaft 52 (STD) which means the intake valve was closed 52 CA after the bottom dead center (BDC). 5, 10 and 15 CA retarding were conducted with camshaft 57 (C57), camshaft 62 (C62) and camshaft 67 (C67).

In order to apply the Miller cycle into the diesel engine three different cam shafts were manufactured and mounted into the engine one by one. The picture of the cam shafts and technical drawing are given in Fig. 1. In order to measure brake torque, the engine is coupled with an electric dynamometer of 20 kW absorbing capacity using an "S" type load cell with the precision of 0.01 kg.

In order to measure species of the exhaust emissions, MRU Spectra 1600 L type gas analyzer has been used. CO, NO, and HC emissions have been obtained as unit of (%) and ppm.

In the study, in-cylinder pressure has been measured by Kistler brand 6061B model, piezo-electric sensor and Kistler 5018 type charge amplifier. The data transfer have been carried out by SMETEC brand data card which has 1 Mbyte data signaling rate from single channel "Combi Combustion Indication System". The angular position of the piston with respect to crank angle has been acquired using Koyo TRD J1000-RZ type encoder which has 1000 pulse/revolution.

The experiments were performed at variable engine speeds 1500, 1800, 2100, 2400, 2700 and 3000 rpm, at full load and under steady-state conditions. In order to compare, standard camshaft was used at initial and then the other camshafts which provide the Miller cycle were mounted into the engine. The experiments were repeated three times for each camshaft, performance and emission data were compared with those of standard camshaft. Total uncertainties of the measured parameters are substantial to verify the accuracy of the test results, so they are indicated in Table 2.

Table 1
Engine properties.

Engine type	Antor (naturally aspirated)
Bore (mm)	85
Stroke (mm)	90
Cylinder number	1
Displacement volume (dm^3)	0.51
Power (kW/rpm)	9/2700
Injection pressure (bar)	175
Injecting timing bTDC (crank angle)	28
Compression ratio	17.5
Maximum engine speed (rpm)	3000
Cooling	Air
Injection	Direct injection

2.2. Theoretical model

Combustion simulation of diesel engine is conducted by using two-zone combustion model to calculate NO emission, torque, brake power, brake efficiency and specific fuel consumption. In this two-zone combustion model [9,19,21,29], the gas region is divided in two zone as burned and unburned gas regions.

The injected fuel reacts with the air in the unburned region and becomes a part of the burned gas region by combustion. In the cylinder, the equation of the energy conservation in differential form may be given as:

$$m\frac{du}{d\theta}+u\frac{dm}{d\theta}=-\frac{dQ_b}{d\theta}-\frac{dQ_u}{d\theta}-P\frac{dV}{d\theta}+\frac{dm_{\mathrm{fi}}}{d\theta}h_{\mathrm{fi}}-\frac{dm_l}{d\theta}h_l \tag{1}$$

where m_l is leak mass and m_{fi} is mass of injected fuel; h_{fi} and h_l are enthalpies of fuel injected and leak mass respectively. The first term of the left side of the equation is the internal energy rate and the second term is the mass rate depending on crank angle. The heat transfers from burned and unburned zone are expressed, respectively as:

$$\dot{Q}_b=h_{\mathrm{tr}}A_bT_{\mathrm{bw}} \tag{2}$$

$$\dot{Q}_u=h_{\mathrm{tr}}A_uT_{\mathrm{uw}} \tag{3}$$

where $T_{\mathrm{uw}}=T_u-T_w$ and $T_{\mathrm{bw}}=T_b-T_w$,, h_{tr} is heat transfer coefficient of burned and unburned gas zones, A_b and A_u are the areas of burned and unburned gas inside the cylinder which are in contact with the cylinder walls and T_b, T_u and T_w are the temperatures of the burned gas zone, unburned gas zone and cylinder walls [22]. The change of stroke volume depending on crank angle is:

$$\frac{dV}{d\theta}=\frac{\pi}{8}B^2S\sin\theta\left[1+\varepsilon\frac{\cos\theta}{\left(1-\varepsilon^2\sin^2\theta\right)^{\frac{1}{2}}}\right] \tag{4}$$

In order to solve the differential equations, the following expressions are used in the model. Internal energy:

$$u=u[T,P,\phi] \tag{5}$$

$$\frac{du}{d\theta}=C_p-\frac{Pv}{T}\left(\frac{\partial\ln v}{\partial\ln T}\right)_P\frac{dT}{d\theta}-v\left[\frac{\partial\ln v}{\partial\ln T}+\frac{\partial\ln v}{\partial\ln P}\right]_T\frac{dP}{d\theta}+\frac{\partial u}{\partial\phi}\frac{d\phi}{d\theta} \tag{6}$$

The burned gas leaking through the rings:

$$\frac{dm_l}{d\theta}=\frac{Cm}{\omega} \tag{7}$$

where C is blow by coefficient which stands for the loss gas by leaking through the rings and ω is angular velocity. The mass balance inside the cylinder can be expressed as:

$$m=m_a+m_{\mathrm{fi}} \tag{8}$$

where m_a and m_{fi} are the masses of the air and injected fuel respectively. If the Eq. (8) is written in differential form, it becomes:

$$\frac{dm}{d\theta}=\frac{dm_a}{d\theta}+\frac{dm_{\mathrm{fi}}}{d\theta} \tag{9}$$

The air and injected fuel rates changing with crank angle within the cylinder are expressed respectively as:

$$\frac{dm_a}{d\theta}=\frac{-\dot{m}_l/\omega}{1+\phi F_{\mathrm{st}}}=\frac{-Cm_a}{\omega} \tag{10}$$

$$\frac{dm_{\mathrm{fi}}}{d\theta}=\frac{1}{\omega}\left(\dot{m}_{\mathrm{fi}}-\frac{\dot{m}_l\phi F_s}{1+\phi F_s}\right) \tag{11}$$

where $\dot{m}_l$, ϕ and F_s are the time-dependent gas leak rate, the equivalence ratio and the stoichiometric fuel–air ratio by mass,

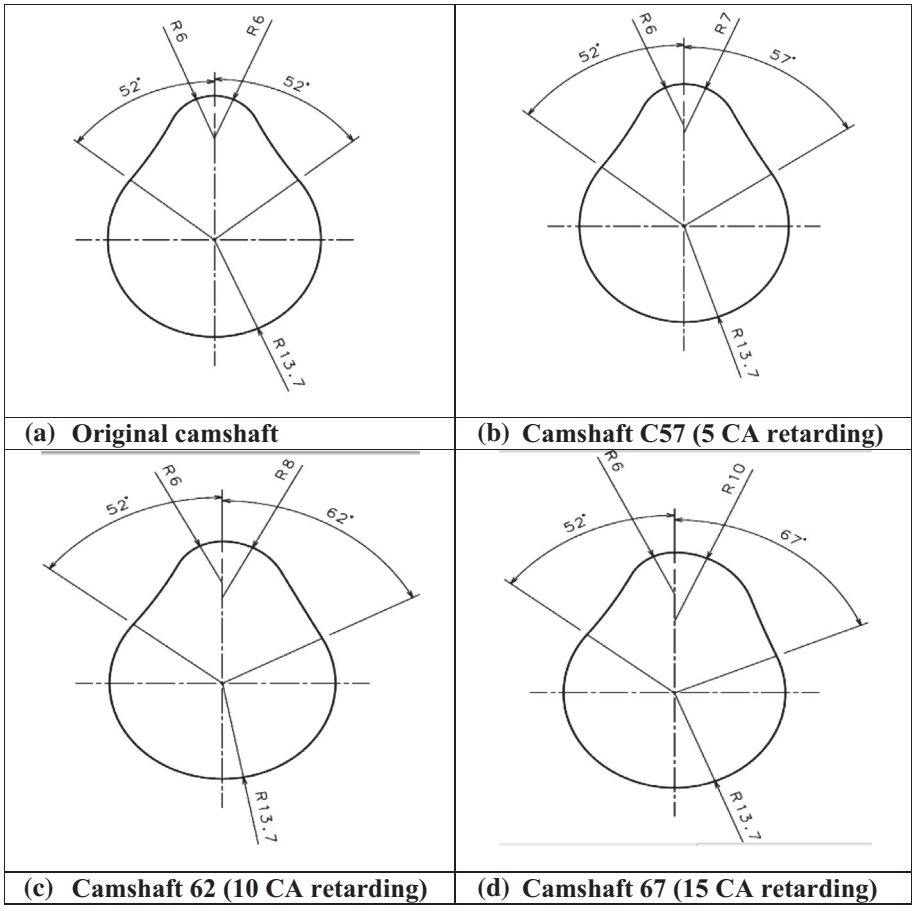

Fig. 1. The technical drawings of the original and modified camshafts in accordance with the Miller cycle.

Table 2
The errors in parameters and total uncertainties.

Parameters	Systematic errors ±
Load (N)	0.1
Speed (rpm)	1.0
Time (s)	0.1
Temperature (°C)	1.0
Fuel consumption (g)	0.01
NO (ppm)	5% of measured value
HC (ppm)	5% of measured value
CO (%)	5% of measured value
SFC (%)	1.5
Torque (Nm)	1.1

respectively. $\dot{m}_{\mathrm{fi}}$ is the time-dependent fuel injected rate and can be expressed as:

$$\dot{m}_{\mathrm{fi}} = \dot{x}_i m_{\mathrm{fi}} \tag{12}$$

where m_{fi} and $\dot{x}_i$ are the total mass of the fuel to be injected and fraction rate of the total injected fuel mass respectively, which can be given as:

$$m_{\mathrm{fi}} = \phi F_{\mathrm{st}}(1 - \mathrm{RGF}) m_a \tag{13}$$

$$\dot{x}_i = \frac{\omega}{\theta_{\mathrm{di}}\Gamma(n)}\left(\frac{\theta - \theta_{\mathrm{si}}}{\theta_{\mathrm{di}}}\right)^{n-1} \exp\left[\frac{-(\theta - \theta_{si})}{\theta_{\mathrm{di}}}\right] \tag{14}$$

where $\Gamma(n)$ is the gamma function [22], θ_{di} is a parameter of injection duration and θ_{si} is the start of fuel injection. The gamma function is derived as:

$$\ln\Gamma(n) = \left(n - \frac{1}{2}\right)\ln(n) - n + \frac{1}{2}\ln(2\pi) + \frac{1}{12n} - \frac{1}{360n^3} + \frac{1}{1260n^5} - \frac{1}{1680n^7} \tag{15}$$

The values of n could be taken for the diesel engine with open chamber as $1 \leqslant n \leqslant 2$ and for divided chamber as $3 \leqslant n \leqslant 5$ but exact value is dependent on fuel used and engine design [22]. Differential equation systems used in the calculation of the processes that consist during the period from the beginning of the compression to the end of the expansion process are given in Eqs. (16)–(27) [9,19,21].

The time (crank angle)-dependent expressions of pressure, burned and unburned gas temperatures, work, heat leak and heat loss are given respectively as:

$$\frac{dP}{d\theta} = \frac{A + B + C}{D} \tag{16}$$

where

$$A = \frac{C}{\omega}\left(\frac{V}{m} + \frac{\vartheta_1}{C_{p,b}T_b}\left((x^2 - x)(h_b - h_u)\right)\right) \tag{17}$$

$$B = \frac{h_{\mathrm{tr}}}{\omega m}A_{\mathrm{cyl}}\left(\sqrt{x}\frac{\vartheta_1}{C_{p,b}T_b}T_{\mathrm{bw}} + (1 - \sqrt{x})T_{\mathrm{uw}}\frac{\vartheta_2}{C_{p,u}T_u}\right) + \left(\frac{\vartheta_1}{C_{p,b}T_b}(h_b - h_u) - (v_b - v_u)\right)\frac{dx}{d\theta} + \frac{1}{m}\frac{dV}{d\theta} + \left(\frac{\vartheta_1}{mC_{p,b}T_b}(xh_b - (1 - x)h_u) - H_u - \frac{V}{m^2}\right)\frac{dm_{\mathrm{fi}}}{d\theta} \tag{18}$$

$$C = (1 - x)\left(\frac{\vartheta_1}{C_{p,b}T_b}\left(-T_u\frac{ds_u}{d\theta} + P\frac{dv_u}{d\theta} + \frac{du_u}{d\theta}\right) - \frac{dv_u}{d\theta} + \frac{\vartheta_2}{C_{p,u}}\frac{ds_u}{d\theta}\right)\frac{d\phi}{d\theta} + x\left(\frac{\vartheta_1}{C_{p,b}T_b}\left(P\frac{dv_b}{d\theta} + \frac{du_b}{d\theta}\right) - \frac{dv_b}{d\theta}\right)\frac{d\phi}{d\theta} \tag{19}$$

$$D = x\left(\frac{\vartheta_1^2}{C_{p,b}T_b} + \frac{\vartheta_3}{P}\right) + (1-x)\left(\frac{\vartheta_2^2}{C_{p,u}T_u} + \frac{\vartheta_4}{P}\right) \tag{20}$$

where

$$\vartheta_1 = \frac{\partial In v_b}{\partial In T_b} v_b, \vartheta_2 = \frac{\partial In v_u}{\partial In T_u} v_u, \vartheta_3 = \frac{\partial In v_b}{\partial In P} v_b, \vartheta_4 = \frac{\partial In v_u}{\partial In P} v_u \tag{21}$$

where x, H_u, A_{cyl} are the burning fraction, lower heating value of fuel and heat transfer area of the cylinder. $C_{p,b}, C_{p,u}; v_b, v_u; s_b, s_u; h_b, h_u$ are specific heat at constant pressure, specific volume, specific entropy and specific enthalpy for the burned and unburned zones respectively.

$$\frac{dT_b}{d\theta} = \frac{1}{C_{p,b}}\left(-\frac{h_{tr}}{\omega m}A_{cyl}\frac{1}{\sqrt{x}}T_{bw} + \vartheta_1\frac{dP}{d\theta}\right) \tag{22}$$

$$\frac{dT_u}{d\theta} = -\frac{h_{tr}}{\omega m C_{pu}}A_{cyl}\frac{T_{uw}}{1+\sqrt{x}} + \frac{\vartheta_2}{C_{pu}}\frac{dP}{d\theta} - \frac{\partial s_b}{\partial \phi}\frac{d\phi}{d\theta}\frac{1}{C_{pb}} \tag{23}$$

$$T_{me} = xT_b + (1-x)T_u \tag{24}$$

$$\frac{dW}{d\theta} = P\frac{dV}{d\theta} \tag{25}$$

$$\frac{dH_l}{d\theta} = \frac{Cm}{\omega}\left[(1-x^2)h_u + x^2 h_b\right] \tag{26}$$

$$\frac{dQ_l}{d\theta} = \frac{h_{tr}}{\omega}A_{cyl}\left[\sqrt{x}T_{bw} + (1-\sqrt{x})T_{uw}\right] \tag{27}$$

The net heat release rate is computed by using the following equation [25]

$$\frac{dQ_n}{d\theta} = P\frac{C_p}{R}\frac{dV}{d\theta} + V\frac{C_p}{R}\frac{dP}{d\theta} \tag{28}$$

Hohenberg [23] gives the coefficient of the heat transfer (h_{tr}) as below:

$$h_{tr} = C_1 V(\theta)^{-0.06} P(\theta)^{0.8}\left(xT_b(\theta) + (1-x)T_u(\theta)\right)^{-0.4}\left(\bar{S}_p + C_2\right)^{0.8} \tag{29}$$

where $V(\theta)$, $P(\theta)$, $T_b(\theta)$ and $T_u(\theta)$ are instantaneous volume, pressure, burned gas and unburned gas temperatures which depend on crank angle. $\bar{S}_p$ is mean piston velocity in meters per second, $C_1 = 130$ and $C_2 = 1.4$ respectively. Sitkei [24] correlation is used to calculate ignition delay and it is written as following:

$$\tau_{id} = 0.5 + 0.1332P(\theta)^{-0.7}e^{\frac{3.92782}{T_u(\theta)}} + 4.637P(\theta)^{-1.8}e^{\frac{3.92782}{T_u(\theta)}} \tag{30}$$

where $P(\theta)$ and $T_u(\theta)$ are time-dependent pressure and time-dependent unburned gas temperature before the injection of fuel. Dual Wiebe function states the burn fraction and x versus crank angle is used to express the heat release from combustion and determined as following [27]:

$$x = a_v\left[Q_{pre}\left(1 - e^{-a_v\left(\frac{\theta}{\theta_{pre}}\right)^{(m_{pre}+1)}}\right) + Q_{dif}\left(1 - e^{-a_v\left(\frac{\theta}{\theta_{dif}}\right)^{(m_{dif}+1)}}\right)\right] \tag{31}$$

where Q_{pre} and Q_{dif} are heat release rate percentages of premixed and diffusive combustion. x is 0 at the beginning of the combustion and x becomes 1 at the end of the combustion. It can be rewritten by differentiating with respect to crank angle:

$$\frac{dx}{d\theta} = a_v\left[\frac{Q_{pre}}{\theta_{pre}}(m_{pre}+1)\left(\frac{\theta}{\theta_{pre}}\right)^{m_{pre}} e^{-a_v\left(\frac{\theta}{\theta_{pre}}\right)^{(m_{pre}+1)}} + \frac{Q_{dif}}{\theta_{dif}}(m_{dif}+1)\left(\frac{\theta}{\theta_{dif}}\right)^{m_{dif}} e^{-a_v\left(\frac{\theta}{\theta_{dif}}\right)^{(m_{dif}+1)}}\right] \tag{32}$$

$$\theta = \theta_r - \theta_b \tag{33}$$

where θ_r and θ_b are reference crank angle and start angle of combustion respectively, a_v, m_{pre}, θ_{pre}, m_{dif}, θ_{dif} are Wiebe constants in the premixed and diffusive combustion conditions.

NO emissions are calculated by using extended Zeldovich mechanism taking into account 10 combustion products including ($CO_2, H_2O, N_2, O_2, CO, H_2, H, O, OH, NO$) [18,21,25–27,29,30]. The three reaction steps of NO formation are used in Table 3 and the rate constant is given as below:

$$k = A_A T^{B_A} e^{\frac{E_A}{T}} \tag{34}$$

The rate of NO formation [mol cm^{-3} s^{-1}] is given as [9,18,21,25–27,29,30]:

$$\frac{d[NO]}{dt} = \frac{2R_1(1-\alpha^2)}{1 + \frac{\alpha R_1}{R_2+R_3}} \tag{35}$$

where $\alpha = \frac{[NO]}{[NO]_e}$ and $[\,]_e$ stands for equilibrium concentration. The other constants written in Eq. (35) are expressed as following:

$$R_1 = k_{+1}[N_2]_e[O_2]_e = k_{-1}[NO]_e[N]_e \tag{36}$$

$$R_2 = k_{+2}[O_2]_e[N]_e = k_{-2}[NO]_e[O]_e \tag{37}$$

$$R_3 = k_{+3}[OH]_e[N]_e = k_{-3}[NO]_e[H]_e. \tag{38}$$

In this study, the ECP code is used developed by Olikara and Borman [28]. The combustion reaction used in the code is expressed as below:

$$\varepsilon\phi(C_\alpha H_\beta O_\gamma N_\delta) + (0.21O_2 + 0.79N_2) \rightarrow v_1CO_2 + v_2H_2O + v_3N_2 + v_4O_2 + v_5CO + v_6H_2 + v_7H + v_8O + v_9OH + v_{10}NO \tag{39}$$

3. Model validation

When we investigate Figs. 2–4, we see that theoretical results agree with experimental data well and there is no considerable error. The maximum error is 4.7% for the engine torque and 5.9% for NO emission. It is clear that torque, brake power, brake efficiency, NO decrease and SFC increase by the application of the Miller cycle with the crankshaft C57. It is seen that in Fig. 4, the model underestimates NO emissions, the reason is that prompt NO formation is neglected, this model just calculates the thermal NO by using Zeldovich mechanism. Also, the measured uncertainty is 5% for NO as can be seen in Table 2. Because of these reasons, it can be said that a good approximation has been obtained between the experimental data and model results in terms of NO prediction.

Table 3
Reactions of NO formation [21].

No.	Reaction	Forward/backward		
		A_A (cm^3/mol s)	B_A	E_A (kcal/mol K)
1	$N_2 + O \leftrightarrow NO + N$	$7.6 \times 10^{13}/1.6 \times 10^{13}$	0/0	−38000/0
2	$O_2 + N \leftrightarrow NO + O$	$6.4 \times 10^{09}/1.5 \times 10^{09}$	0/0	−3150/−19500
3	$OH + N \leftrightarrow NO + H$	$4.1 \times 10^{13}/2 \times 10^{14}$	0/0	0/−23650

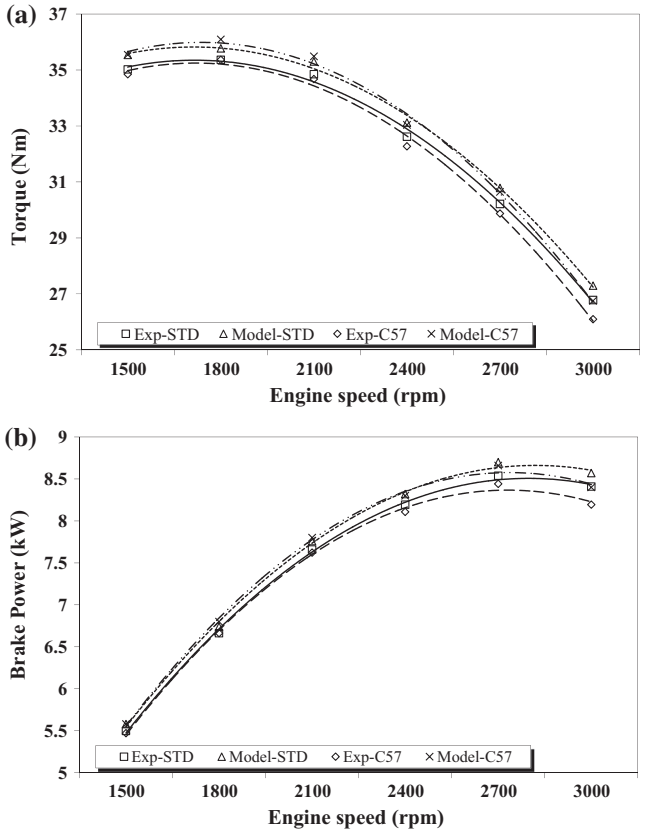

Fig. 2. Comparison of theoretical and experimental data of (a) torque and (b) brake power.

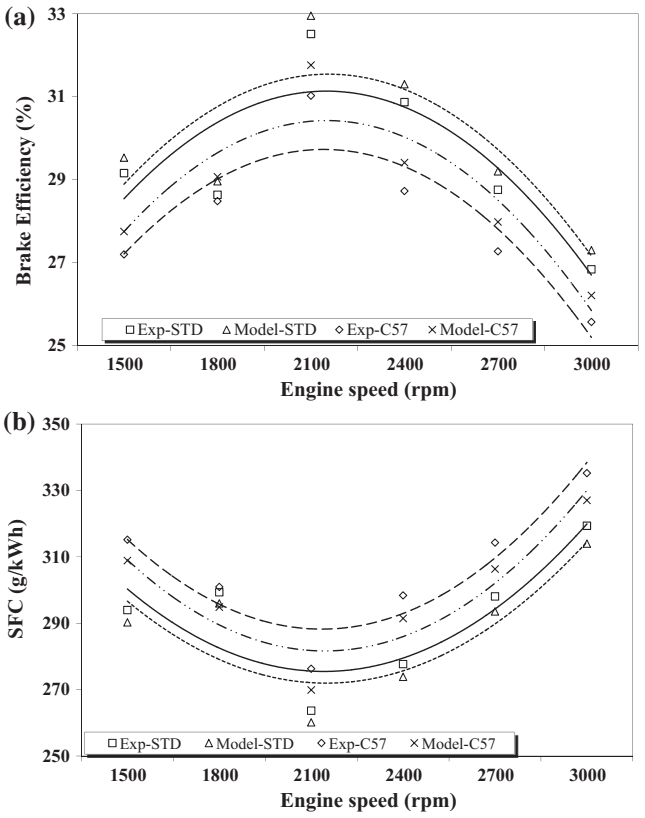

Fig. 3. Comparison of theoretical and experimental data of (a) brake efficiency and (b) SFC.

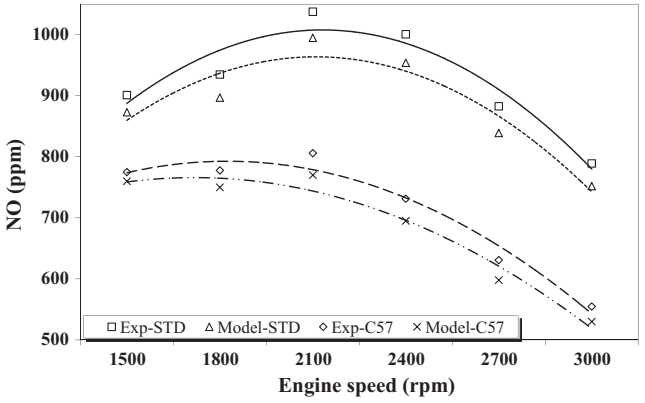

Fig. 4. Comparison of theoretical and experimental data of NO formation.

Figs. 5–7 show the comparison of theoretical and experimental data for cylinder pressures, temperatures and net heat release rates at the maximum torque and brake power conditions. The maximum power conditions are obtained at 2700 rpm and the peak cylinder pressure, temperature and net heat release rate are lower compared to those at the maximum torque conditions. It is obvious that the maximum cylinder pressures and temperatures diminish with the application of the camshaft C57. However, the maximum net heat release rate increase, because ignition delay increases with decreasing peak pressure and temperature as can be clearly seen in Fig. 7. Hereby, more fuel is injected between the duration of injection and ignition, and higher amount of fuel is burned by the ignition in the premixed combustion phase. Due to higher ignition delay with the application of the camshaft C57, the peak values of the combustion pressures, temperatures and net heat release rates shift to the right. If we compare Figs. 4 and 6, we see that NO emissions increase with increasing peak combustion temperatures as expected.

4. Results and discussion

Fig. 8 shows the engine torque and brake power with respect to change of engine speed for different camshafts. As it can be seen from the figures that the engine torque decreases with increasing engine speed, however, the brake power increases until 2700 rpm and then starts to decrease. The main reason of reduction in the torque is decrease of combustion duration and in-cylinder pressures. There is a relation between the brake power and engine speed, the brake power is obtained by multiplying the torque and engine speed. Therefore, the brake power increases while the torque decreases and engine speed increases. The maximum brake power is seen at 2700 rpm. The application of the Miller cycle by the different camshafts reduces the engine torque and brake power at the lower engine speeds, but at the higher engine speeds, they enhance with C62 and C67 camshafts. It is clear that even though the performance decreases with high retarding angles at low engine speeds, it increases with high retarding angles at higher engine speeds. It means that more air mass is introduced into the cylinder at higher retarding angles and higher engine speeds since duration of the suction remains. The maximum reduction rate is seen at 1500 rpm, as 3% and the maximum increase rate is seen at 3000 rpm as 1.5% with C67 for the engine torque and brake power.

Fig. 9 demonstrates the brake efficiency and specific fuel consumption with respect to change of engine speed for different

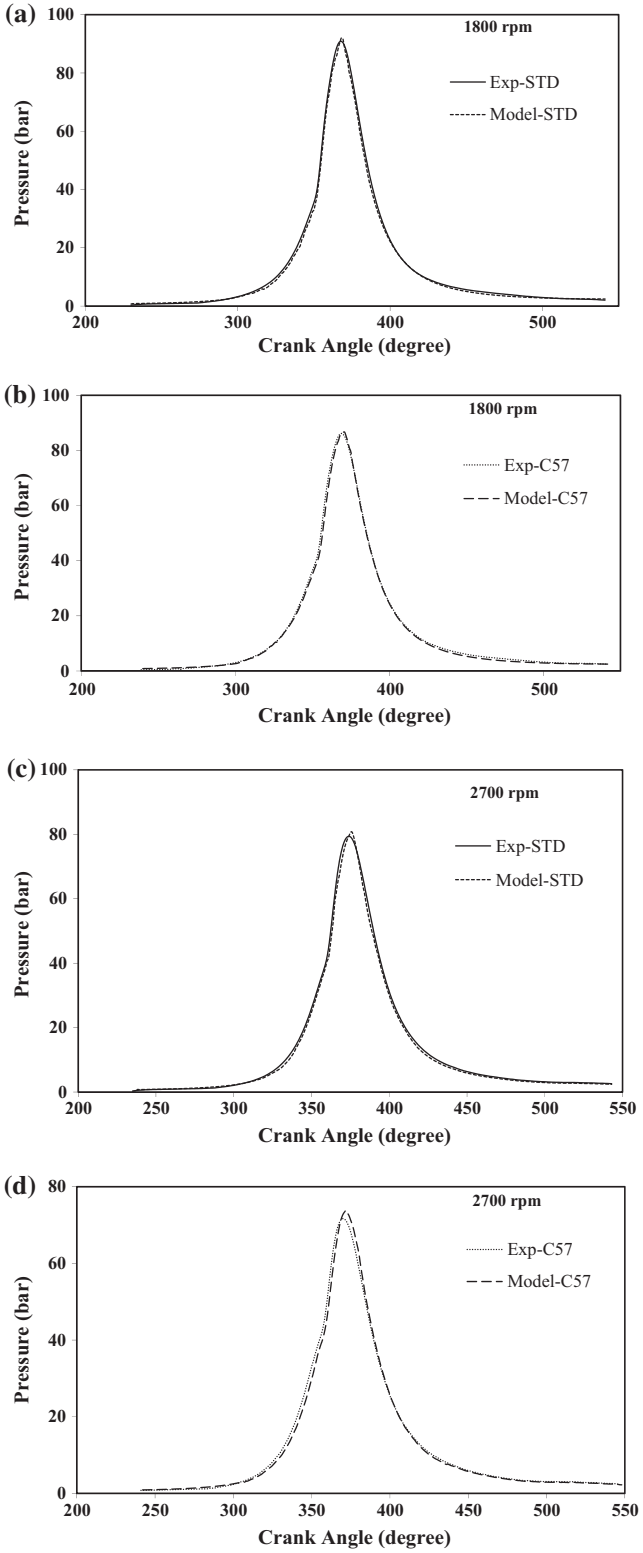

Fig. 5. Comparison of theoretical and experimental data for cylinder pressure for (a) STD, (b) C57 conditions at the maximum torque and (c) STD, (d) C57 at the maximum brake power.

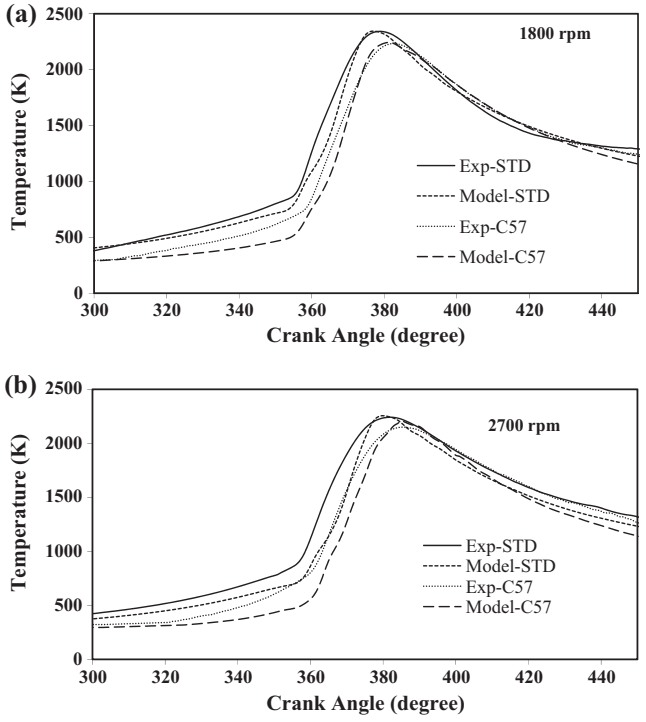

Fig. 6. Comparison of theoretical and experimental data for cylinder temperature at (a) the maximum torque and (b) the maximum brake power.

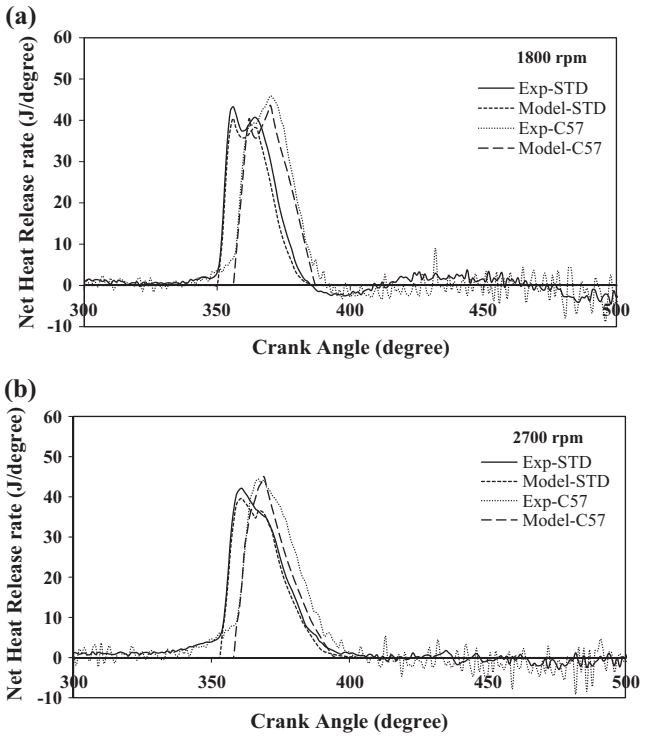

Fig. 7. Comparison of theoretical and experimental data for heat release rate at (a) the maximum torque and (b) the maximum brake power.

camshafts. It is clear from the figures that middle engine speeds provide the maximum brake efficiency and minimum specific fuel consumption. At the low and high engine speeds, lower brake efficiency and higher specific fuel consumption are seen. At the lower engine speeds, the application of the Miller cycle affects negatively the brake efficiency and SFC, however, at the higher engine speeds such as 2700 and 3000 rpm, the brake efficiency increases while the specific fuel consumption reduces with C67 camshaft as more air mass is sucked into the cylinder. It should be noted that a reduction trend is seen in the brake efficiency with the application

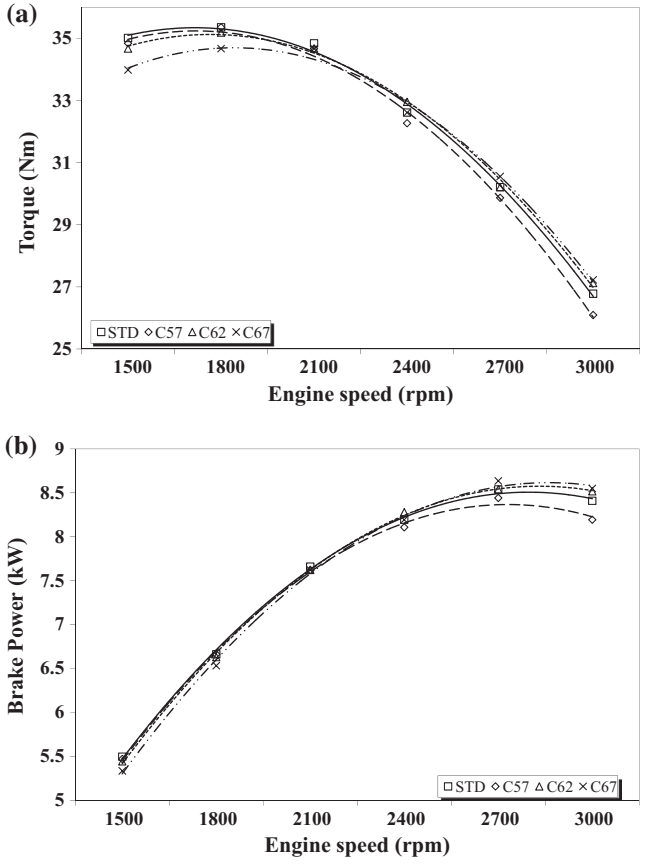

Fig. 8. The variation of (a) torque and (b) brake efficiency with respect to engine speed for different camshafts.

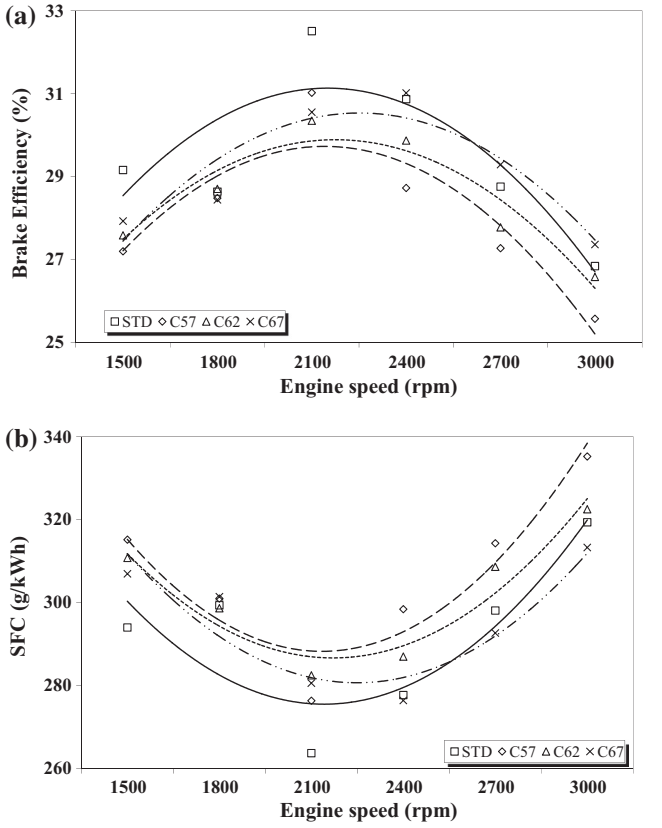

Fig. 9. The variation of (a) brake efficiency and (b) specific fuel consumption with respect to engine speed for different camshafts.

of the Miller cycle. The maximum reduction and increase in the brake efficiency are 6.7% with C57 at 1500 rpm and 1.9% with C67 at 3000 rpm, respectively. The maximum increment and decrease in the specific fuel consumption are 7.2% with C57 and 1.8% with C67, respectively.

The variation of NO with respect to engine speed is depicted in Fig. 10. It is well known in the open literature that NO emissions are very sensitive to combustion temperature and duration [26,27,29–31]. The combustion temperature and duration affect the formation of NO emissions, negatively. Also the combustion temperature is affected by equivalence ratio. The maximum combustion temperature and NOx concentration are seen about equivalence ratio is 1. However, the diesel engines generally run with lean charge and the maximum equivalence ratio of the test engine is about 0.9 and it is reached in the middle ranges of the engine speeds. The higher NOx is seen with the higher combustion duration. It can be said that in-cylinder temperatures are lower, although the combustion duration is longer at the low engine speeds. However, even though the combustion temperatures are higher, the combustion duration is lower at the high engine speeds. The maximum combustion temperatures are reached in the middle engine speeds. Therefore, NO formation reaches to the maximum concentration. The camshafts which provide delayed closure of the intake valve give lower NO emissions compared to standard camshaft at all engine speeds. The highest and lowest NO reduction rates are seen as 30% with C57 at 3000 rpm and as %7 with C62 at 2100 rpm, respectively. The minimum NO is found as 550 ppm with C57 at 3000 rpm.

The variation of HC with respect to engine speed is illustrated in Fig. 11. HC emissions are incomplete combustion products and they increase at rich charge and cold operating conditions. HC emissions decrease with increasing oxygen concentration and combustion temperatures. It is obviously seen that HC formation rate decreases with increasing engine speeds since in-cylinder charge gets leaner and combustion temperatures increase. HC emissions generally show increase trend due to increase of incomplete combustion rate with the application of the Miller cycles. The oxygen concentration of the cylinder charge and combustion temperatures decrease with the Miller cycle. Therefore, as expected, the HC concentration increases. The highest and lowest increase rates are 38% with C67 at 2400 rpm and 2% with C62 at 2100 rpm, respectively. The maximum and minimum reduction rates are 11% with C57 at 1500 rpm and 1% with C57 at 1800 rpm. The maximum HC is 137 ppm with C57 at 1500 rpm and the minimum HC is 59 ppm with C62 at 3000 rpm.

The variation of CO with respect to engine speed is demonstrated in Fig. 12. The formation characteristics of CO is similar to those of HC emissions, therefore CO formation rate abates with increasing engine speeds. The formation of CO and HC emissions strongly depends on oxygen concentration (equivalence ratio) of the cylinder charge rather than temperature. They increase at the lower oxygen concentration. Because, the Carbon in the fuel does react with insufficient oxygen, so more CO is formed instead of the formation of CO_2. Also the in-cylinder gas temperature is affected by oxygen concentration, it raises with the increasing oxygen concentration, thus, the formation rate of CO_2 rises up as the CO diminishes. It is seen that there are no considerable differences between the results of the different camshaft applications in middle range of the engine speeds. At lower engine speeds such as 1500 and 1800 rpm, CO emissions abate with the application of the Miller camshafts. However, CO emissions increase with C57 at the higher engine speeds such as 2700 and 3000 rpm. The highest increase and decrease rates are 18% with C57 at 3000 rpm and 11% with C62 at 3000 rpm, respectively.

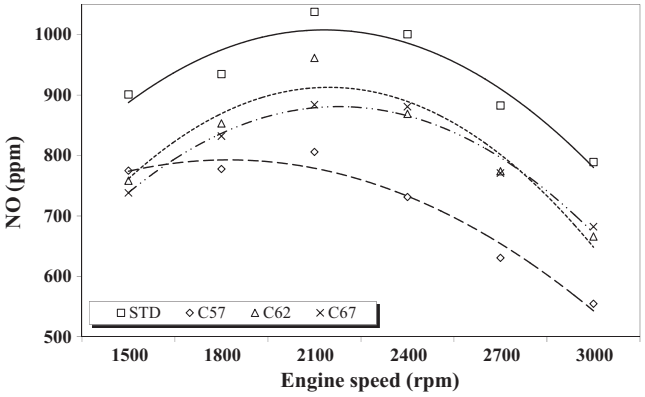

Fig. 10. The variation of NO emissions with respect to engine speed for different camshafts.

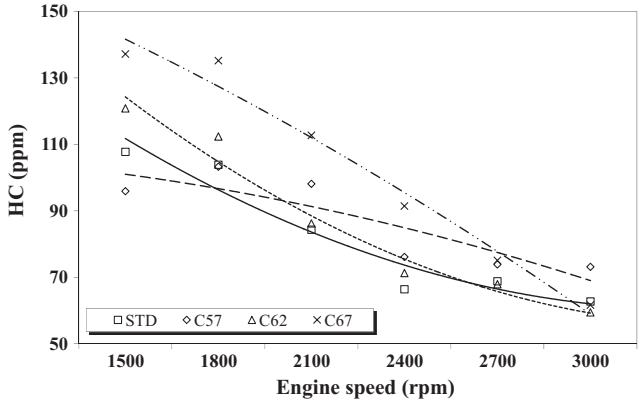

Fig. 11. The variation of HC emissions with respect to engine speed for different camshafts.

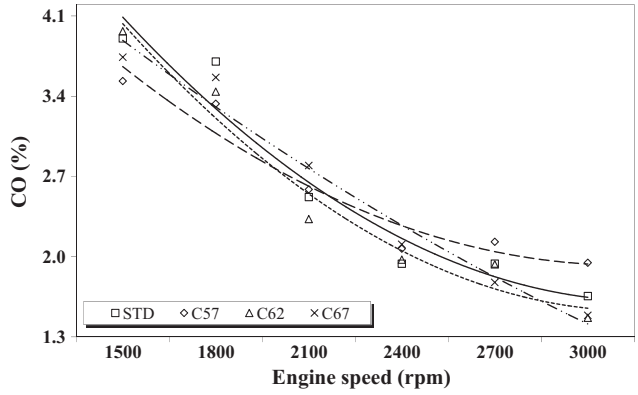

Fig. 12. The variation of CO emissions with respect to engine speed for different camshafts.

The maximum and minimum CO emissions are obtained as 3.97% with C62 at 1500 rpm and 1.47% with C62 at 3000 rpm.

5. Conclusion

This study reports the influences of the Miller cycle application into a diesel engine in terms the performance and emission outputs. An experimental and theoretical study has been conducted in order to investigate the performance and emission parameters. Theoretical study has been performed by using two-zone combustion model. Theoretical model results have been verified with non-remarkable errors in terms of torque, brake power and efficiency, SFC and NO emissions. The maximum error is less than 6%.

An improvement in torque, brake power and efficiency and SFC has seemed with the camshaft C62 and C67 at higher engine speeds such as 2700 and 3000 rpm. However, these performance parameters are worsened at the lower engine speeds and with the application of the camshaft C57 because of charge loss and reduction in the volumetric efficiency. However, NO emissions decrease at all engine speeds. The maximum increase rates are seen with the C67 at 3000 rpm, as 1.5% and 2% in the torque and brake efficiency, respectively. At this condition, the reduction rates of NO, HC and CO emissions are 14%, 2% and 10%, respectively. The maximum NO reduction rate is obtained as 30% with the C57 at 3000 rpm. On the other hand, at this condition, the torque and brake efficiency decrease by 2.5% and 4.5%, respectively. HC and CO emissions do not change considerably. Consequently, the application of the Miller cycle remarkably decreases NO emissions. Therefore, this method with modified camshafts could be used in the diesel engines owing to its lower cost and easy application.

Acknowledgements

This study is a part of PhD thesis of the first author. The authors thank The Scientific and Technological Research Council of Turkey (TUBITAK- the project number is 111M065), Yildiz Technical University Scientific Research Projects Coordination Department (the project number is 2011-10-01-KAP03) and Turkish Academy of Sciences (TUBA) for their financial supporting.

References

[1] Al-Sarkhi A, Akash BA, Jaber JO. Efficiency of miller engine at maximum power density. Int Commun Heat Mass 2002;29:1159–67.
[2] Al-Sarkhi A, Jaber JO, Probert SD. Efficiency of a Miller engine. Appl Energy 2006;83:343–51.
[3] Al-Sarkhi A, Al-Hinti I, Abu-Nada E, Akash B. Performance evaluation of irreversible Miller engine under various specific heat models. Int Commun Heat Mass 2007;34:897–906.
[4] Zhao Y, Chen J. Performance analysis of an irreversible Miller heat engine and its optimum criteria. Appl Therm Eng 2007;27:2051–8.
[5] Wu C, Puzinauskas PV, Tsai JS. Performance analysis and optimization of a supercharged Miller cycle Otto engine. Appl Therm Eng 2003;23:511–21.
[6] Lin JC, Hou SS. Performance analysis of an air-standard Miller cycle with considerations of heat loss as a percentage of fuel's energy, friction and variable specific heats of working fluid. Int J Therm Sci 2008;47:182–91.
[7] Ebrahimi. Thermodynamic modeling of performance of a Miller cycle with engine speed and variable specific heat ratio of working fluid. Comput Math Appl 2011;62:2169–76.
[8] Ebrahimi. Performance analysis of an irreversible Miller cycle with considerations of relative air–fuel ratio and stroke length. Appl Math Model 2012;36:4073–9.
[9] Gonca G. Investigation of the effect of steam injection on performance and emissions in a turbocharged diesel engine running with the Miller cycle, PhD Thesis, 2013.
[10] Gonca G, Sahin B, Ust Y. Performance maps for an air-standard irreversible Dual-Miller cycle (DMC) with late inlet valve closing (LIVC) version. Energy 2013;5:285–90.
[11] Wang Y, Lin L, Zeng S. Application of the Miller cycle to reduce NOx emissions from petrol engines. Appl Energy 2008;85:463–74.
[12] Wang Y, Lin L, Roskilly AP. An analytic study of applying Miller cycle to reduce NOx emission from petrol engine. Appl Therm Eng 2007;27:1779–89.
[13] Mikalsen R, Wang YD, Roskilly AP. A comparison of Miller and Otto cycle natural gas engines for small scale CHP applications. Appl Energy 2009;86:922–7.
[14] Kesgin U. Efficiency improvement and NOx emission reduction potentials of two-stage turbocharged Miller cycle for stationary natural gas engines. Int J Energy Res 2005;29:189–216.
[15] Li T, Gao Y, Wang J, Chen Z. The Miller cycle effects on improvement of fuel economy in a highly boosted, high compression ratio, direct-injection gasoline engine: EIVC vs. LIVC. Energy Convers Manage 2014;79:59–65.
[16] Wang Y, Zeng S, Huang J. Experimental investigation of applying Miller cycle to reduce NOx emission from diesel engine. Proc. IMechE, Part A: J. Power Energy 2005;219:631–8.
[17] Gonca G, Kayadelen HK, Safa A. Comparison of diesel engine and Miller cycled diesel engine by using two zone combustion model. 1. In: INTNAM Symp 2011;17:681–97.

[18] Gonca G, Sahin B, Ust Y, Parlak A. A study on late intake valve closing miller cycled diesel engine. Arab J Sci Eng 2013;38:383–93.
[19] Gonca G, Sahin B, Ust Y, Parlak A, Safa A. Comparison of steam injected diesel engine and miller cycled diesel engine by using two zone combustion model. J Energy Inst, in press. http://dx.doi.org/10.1016/j.joei.2014.04.007.
[20] Rinaldini CA, Mattarelli E, Golovitchev VI. Potential of the Miller cycle on a HSDI diesel automotive engine. Appl Energy 2013;112:102–19.
[21] Gonca G. Investigation of the effects of steam injection on performance and NO emissions of a diesel engine running with ethanol–diesel blend. Energy Convers Manage 2014;77:450–7.
[22] Ferguson R. Internal combustion engines applied thermosciences. New York: John Wiley & Sons Inc.; 1986.
[23] Hohenberg G. Advanced approaches for heat transfer calculations. SAE J Automot Eng 1979:790825. http://dx.doi.org/10.4271/790825.
[24] Sitkei G. Kraftstoffaufbereitung und verbrennung bei dieselmotoren. Berlin: Springer Verlag; 1964.
[25] Heywood JB. Internal combustion engine fundamentals. New York: McGraw-Hill Inc.; 1998.
[26] Cesur I, Parlak A, Ayhan A, Boru B, Gonca G. The effects of electronic controlled steam injection on spark ignition engine. Appl Therm Eng 2013;55:61–8.
[27] Kokkulunk G, Gonca G, Ayhan V, Cesur I, Parlak A. Theoretical and experimental investigation of diesel engine with steam injection system on performance and emission parameters. Appl Therm Eng 2013;54:161–70.
[28] Olikara C, Borman G. A computer program for calculating properties of equilibrium combustion products with some applications to the engines. SAE J Automot Eng 1975:750468.
[29] Kökkülünk G, Parlak A, Ayhan V, Cesur I, Gonca G, Boru B. Theoretical and experimental investigation of steam injected diesel engine with EGR. Energy 2014;74:331–9.
[30] Kökkülünk G, Gonca G, Parlak A. The effects of design parameters on performance and NO emissions of steam injected diesel engine with exhaust gas recirculation. Arab J Sci Eng 2014;39:4119–29. http://dx.doi.org/10.1007/s13369-014-0984-z.
[31] Gonca G, Sahin B, Ust Y, Parlak A. Determination of the optimum temperatures and mass ratios of steam injected into turbocharged internal combustion engines. J Renew Sustainable Energy 2013;5:023119. http://dx.doi.org/10.1063/1.4798313.